NEUROSCIENCE

Locally sequential synaptic reactivation during hippocampal ripples

Tomoe Ishikawa[1] and Yuji Ikegaya[1,2]*

The sequential reactivation of memory-relevant neuronal ensembles during hippocampal sharp-wave (SW) ripple oscillations reflects cognitive processing. However, how a downstream neuron decodes this spatiotemporally organized activity remains unexplored. Using subcellular calcium imaging from CA1 pyramidal neurons in ex vivo hippocampal networks, we discovered that neighboring spines are activated serially along dendrites toward or away from cell bodies. Sequential spine activity was engaged repeatedly in different SWs in a complex manner. In a single SW event, multiple sequences appeared discretely in dendritic trees, but overall, sequences occurred preferentially in some dendritic branches. Thus, sequential replays of multineuronal spikes are distributed across several compartmentalized dendritic foci of a postsynaptic neuron, with their spatiotemporal features preserved.

INTRODUCTION

Neuronal activity in the central nervous system is coordinated by transient sequences of action potentials across neuronal ensembles (*1*–*7*), which may be defined by intrinsic wiring patterns of their neuronal microcircuits. Anatomical evidence indicates that presynaptic CA3 neurons in the hippocampus are connected with postsynaptic CA1 neurons in a subcellularly nonrandom manner (*8*). In the visual cortex, neuron populations that share common receptive fields are interconnected through clustered synapses (*9*). Therefore, spikes of a presynaptic neuron population may converge, at least in part, on the dendritic foci of a single neuron. Adjacent spines receive synchronous synaptic inputs under spontaneously ongoing network activity (*10*, *11*). However, how multineuronal spike sequences activate postsynaptic neurons remains to be mapped at a subcellular level with high temporal resolution.

Dendrites integrate the spatiotemporal dynamics of synaptic inputs through their electrically active cable properties and ion channels (*12*–*14*). The sequential activation of clustered spines induces nonlinear dendritic summations and modifies their impacts on postsynaptic potentials (*15*, *16*). However, in many studies on dendritic integration, synapses have been artificially stimulated under experimental control. Moreover, existing dendritic imaging studies have had insufficient video frame rates to dissect the sequential structures of synaptic inputs; therefore, little is known regarding how naturally occurring spike sequences excite postsynaptic dendrites.

In the present work, we investigated how the dendrites of CA1 pyramidal cells are spatiotemporally activated during spontaneous sharp-wave (SW) ripple oscillations. During SWs, the offline reactivation of spatial and episodic neuronal sequences is observed in the hippocampus (*4*–*7*), and this reactivation contributes to memory consolidation (*17*) and neuronal homeostasis (*18*). We used hippocampal slice cultures because they have low light scattering and provide a unique opportunity for high-speed, large-scale optical recordings of spontaneous calcium activity from hundreds of spines (*11*). In these ex vivo preparations, hippocampal networks self-reorganize to emit spontaneous neuronal activity that resembles in vivo neuronal activity (*19*), which includes SWs with repeated spike sequences (*20*, *21*). We found that neurons that fired spikes frequently in SWs received transient synaptic inputs during SWs. The synaptic barrages during SWs were composed of a rich repertoire of sequential structures. Moreover, sequential synaptic inputs produced vectorial spine activation in the IN or OUT direction according to the dendritic branch. Our data suggest that sequential spikes of hippocampal memory engrams may excite neighboring spines of a postsynaptic neuron in a different order, which may reflect forward or reverse activity replays.

RESULTS

SW-participating CA1 pyramidal cells increase synaptic activity during SWs

The mean event frequency of SWs in hippocampal slice cultures was 67 ± 44 per minute (mean ± SD of 27 slices). Spectrogram analyses of local field potentials (LFPs) recorded from the CA1 stratum pyramidale revealed that the SWs consisted mainly of high-frequency (125 to 250 Hz) and low-frequency (<80 Hz) components (Fig. 1, A and B). Current source density analyses revealed that the SWs were associated with current sinks in the stratum oriens and stratum radiatum (Fig. 1C). Moreover, the SWs were largely abolished by a bath application of carbachol, an acetylcholine receptor agonist (Fig. 1, D and E; $P = 0.015$, $t_4 = 4.1$, paired t test). All these characteristics of ex vivo SWs are consistent with those of in vivo SWs observed in the hippocampus (*22*).

First, we recorded the spikes of 21 CA1 pyramidal cells in the cell-attached configuration (Fig. 2A and fig. S1; $n = 21$ slices). Of these 21 cells, 12 cells (57%) emitted spikes that were more time-locked to SWs than predicted by a Poissonian stochastic process (Fig. 2, B and C). We classified those 12 cells as SW participants, whereas the other 9 cells were classified as nonparticipants. SW participants and nonparticipants did not differ in their basic electrical or morphological properties, such as membrane capacitances ($P = 0.83$, $t_{19} = 0.21$, Student's t test), membrane resistances ($P = 0.58$, $t_{19} = 0.57$, Student's t test), or spine densities ($P = 0.30$, $t_{21} = 1.01$, Student's t test), or in their baseline spike rates ($P = 0.32$, $t_{19} = 1.01$, Student's t test); only SW participants showed transiently increased spike rates during SWs (Fig. 2, D and E).

Then, we moved to the whole-cell configuration and intracellularly loaded the neurons with the fluorescent calcium indicator Fluo-4

[1]Graduate School of Pharmaceutical Sciences, The University of Tokyo, Tokyo 113-0033, Japan. [2]Center for Information and Neural Networks, National Institute of Information and Communications Technology, Suita City, Osaka 565-0871, Japan. *Corresponding author. Email: yuji@ikegaya.jp.

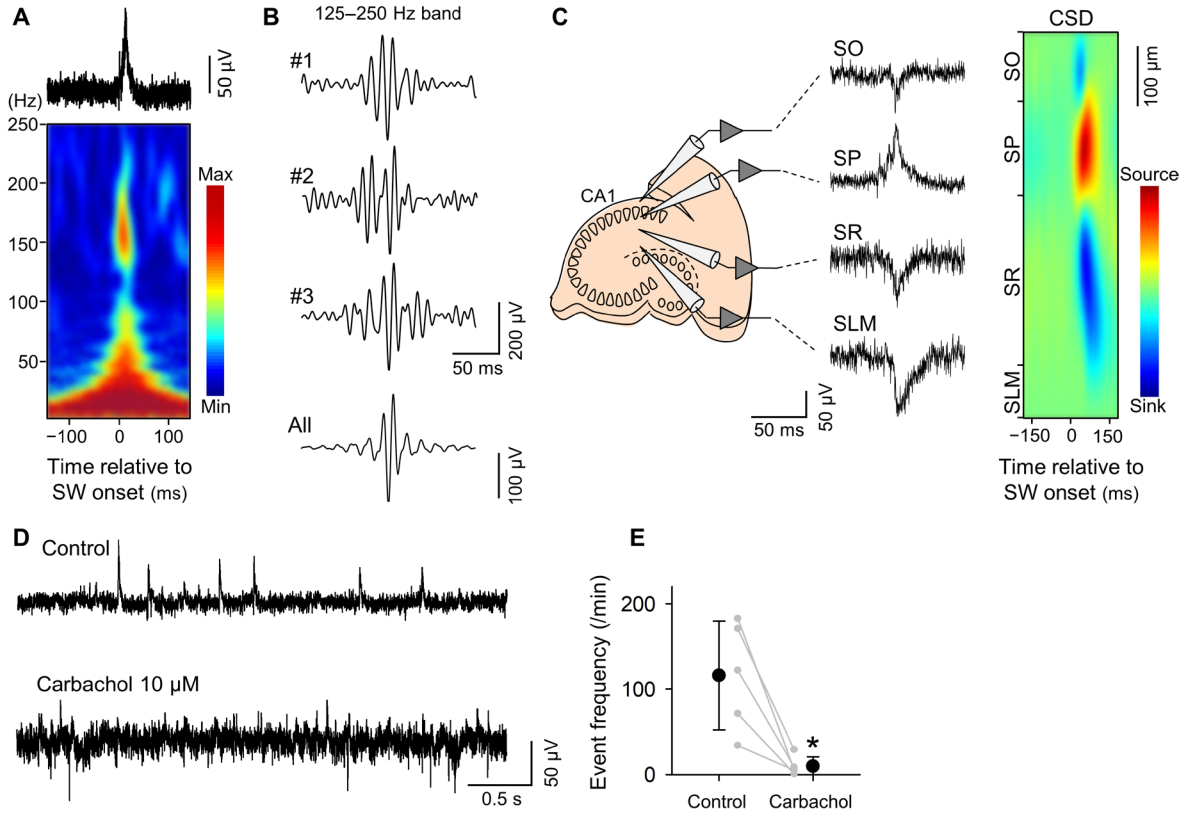

Fig. 1. Cultured hippocampal networks spontaneously emit SWs. (**A**) An example trace of LFPs recorded from the CA1 stratum pyramidale during a SW event (top) was analyzed using the wavelet transform (bottom). (**B**) Three representative 125 to 250 Hz filtered SW traces and the average of all 1048 SWs recorded in a slice. (**C**) Left: A SW event was captured in LFPs of the CA1 stratum oriens (SO), the stratum pyramidale (SP), the stratum radiatum (SR), and the stratum lacunosum moleculare (SLM). Right: The current source density (CSD) was calculated for the average traces of 20 consecutive SWs. (**D**) Representative traces of SWs recorded from the CA1 stratum pyramidale before and 10 min after bath application of 10 μM carbachol. (**E**) Carbachol reduced the event frequency of SWs ($n = 5$ slices; $^*P = 0.015$, $t_4 = 4.1$, paired t test).

(Fig. 2F). Using a spinning disk confocal microscope that covered a visual field of 187 μm × 122 μm, we imaged 233 ± 72 spines per cell (mean ± SD of 23 videos taken from 21 cells, ranging from 118 to 385 spines) from basal or proximal oblique dendrites at a frame rate of 100 Hz for 30 to 120 s (fig. S2). The membrane potential was clamped at −30 mV to reliably detect synaptic calcium events. Because voltage clamping does not affect the frequency of somatic excitatory postsynaptic current (*23*), it is unlikely to have a substantial influence on the level of local synaptic inputs per se. Under these conditions, spines exhibited spontaneous calcium transients (Fig. 2G), which were abolished by 50 μM D-2-amino-5-phosphonopentanoic acid (AP5), an *N*-methyl-D-aspartate (NMDA) receptor antagonist (*23*). Although there was no difference in spike output rates, SW participants had higher frequencies of baseline calcium activity per spine than nonparticipants (Fig. 2, H to J; $P = 0.0020$, $t_{19} = 3.6$, Welch's t test; compare Fig. 2, C and D). The amplitudes of calcium activity observed in SW participants were also significantly larger than those in nonparticipants (5.1 ± 2.8% versus 3.8 ± 1.6%, mean ± SD of SW participant and nonparticipant; $P = 2.44 \times 10^{-81}$, $t_{2309} = 19.9$, Welch's t test). In SW participants, calcium activity gradually increased approximately 400 ms before SWs and reached a peak during SWs (Fig. 2H). This time course was consistent with pre-SW gradual depolarizations of in vivo CA1 pyramidal cells (*24*). In nonparticipants, calcium activity also increased before SWs but did not peak during SWs (Fig. 2I). As a result, the increases in calcium activity in SW participants were larger than those in nonparticipants, particularly between 300 and 0 ms before SW occurrence (Fig. 2J).

We examined the spatial organization of SW-relevant spine activity in SW participants. The locations of spines were three-dimensionally determined, and the path distances (d_{ij}) between spines i and j that were coactivated within a time window of 20 ms were measured along dendritic axes. As the degree of spatial clustering, we computed the geometric energy $\Sigma 1/d_{ij}$ for all pairs of spines activated in every time window (*25*). The geometric energy increased around the SW periods only in SW participants (Fig. 2, K and L), suggesting that adjacent spines are recruited in SWs in SW participants but not in nonparticipants. Because the geometric energy values may be sensitive to outliers, we introduced another index that focused only on nearby spines—the total number of pairs of coactivated spines within 10 μm of each other at a given time. This parameter again confirmed that SWs recruited adjacent spines only in SW participants (fig. S3). Incidentally, we previously confirmed that clustered activity does not result from multiple synaptic contacts made by the same presynaptic axons (*11*).

SW participants receive sequential synaptic inputs during SWs

Because the sequential activity of memory-relevant neurons repeats during SWs (*4*–*7*), we searched for repetitions of sequential spine activity. We created a series of binary matrices representing the spatiotemporal

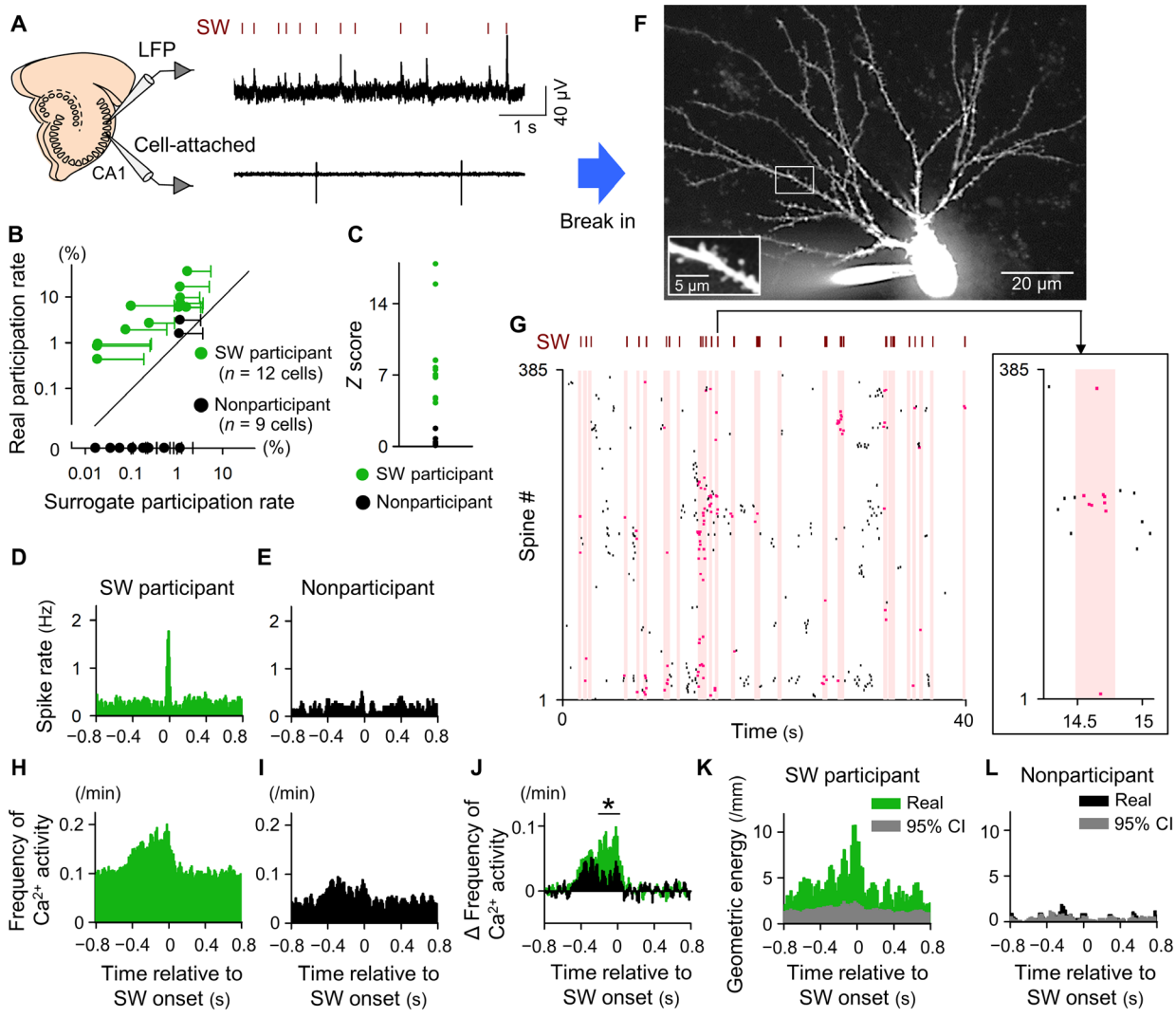

Fig. 2. SW-participating CA1 pyramidal cells receive clustered synaptic inputs during SWs. (**A**) Representative traces for simultaneous recordings of LFPs from the stratum pyramidale and spikes from a cell-attached recording of a CA1 pyramidal cell in a cultured hippocampal slice. Red tick marks in the top row indicate the SW times detected in the LFP trace. (**B**) The participation rates, i.e., the probabilities that SWs were accompanied by spikes of a given neuron, are plotted versus their chance levels estimated from 10,000 surrogates, in which the Poisson point process generated the same number of spikes in each cell. Each circle indicates the mean value of a single cell, and its error bar represents the 95% confidence interval of the surrogates. (**C**) *Z* scores of the spike participation rates in SWs of individual cells. Green dots indicate SW participants, and black dots indicate nonparticipants. (**D** and **E**) Peri-SW time histograms of the mean spike rates of 12 SW participants (D) and 9 nonparticipants (E). (**F**) Stack image of basal dendrites of a CA1 pyramidal cell filled with Fluo-4. (**G**) Representative raster plot of calcium transients emitted by a total of 385 imaged spines. Each dot indicates a single event of a single spine. Red dots indicate spine activity that occurred within 300 ms (red shades) before the SW onset (top ticks). A SW event is time-expanded in the right inset. (**H** and **I**) Peri-SW time histograms of the mean rates of calcium activity per spine in SW participants ($n = 14$ movies from 12 cells) (H) and nonparticipants ($n = 9$ movies from 9 cells) (I). (**J**) Peri-SW time histograms of the difference in the frequency of calcium activity from the baseline. Green bars indicate SW participants, and black bars indicate nonparticipants. The black line represents the time frames in which the difference of the calcium activity frequency between participants and nonparticipants is larger than the 95% confidential interval estimated by 10,000 bootstrap surrogates, in which the calcium activity was resampled randomly from the data pooled from both participants and nonparticipants. (**K** and **L**) Peri-SW time histogram of the mean geometric energies (spatial clustering) of synchronously activated spines in 12 SW participants (K) and in 9 nonparticipants (L). The gray histogram indicates the 95% confidence intervals (CI) of 10,000 surrogates, in which the spine locations were randomly exchanged within the videos.

activity of spines for a time window of 300 ms every 10-ms step. The sums of the elements of the Hadamard products between pairs of these matrices with a Gaussian filter ($\sigma = 40$ ms) were regarded as the similarity indexes of the matrix pairs (*26*). If the similarity index exceeded the value when two spines were exactly repeated, then the spatiotemporal pattern of the spine activity shared by the two matrices included a sequence. In this definition, each sequence contained at least three spines and was repeated at least twice. As a result, we found that spontaneous spine activity contained a rich repertoire of repeated sequences (Fig. 3A and fig. S4A). In SW participants, sequential spine activity was statistically significant; that is, sequences appeared more frequently in SW participants than their event-swapped surrogates (fig. S4, B and C). The number of sequences is mathematically expected to increase as a function of the total spine activity level, and

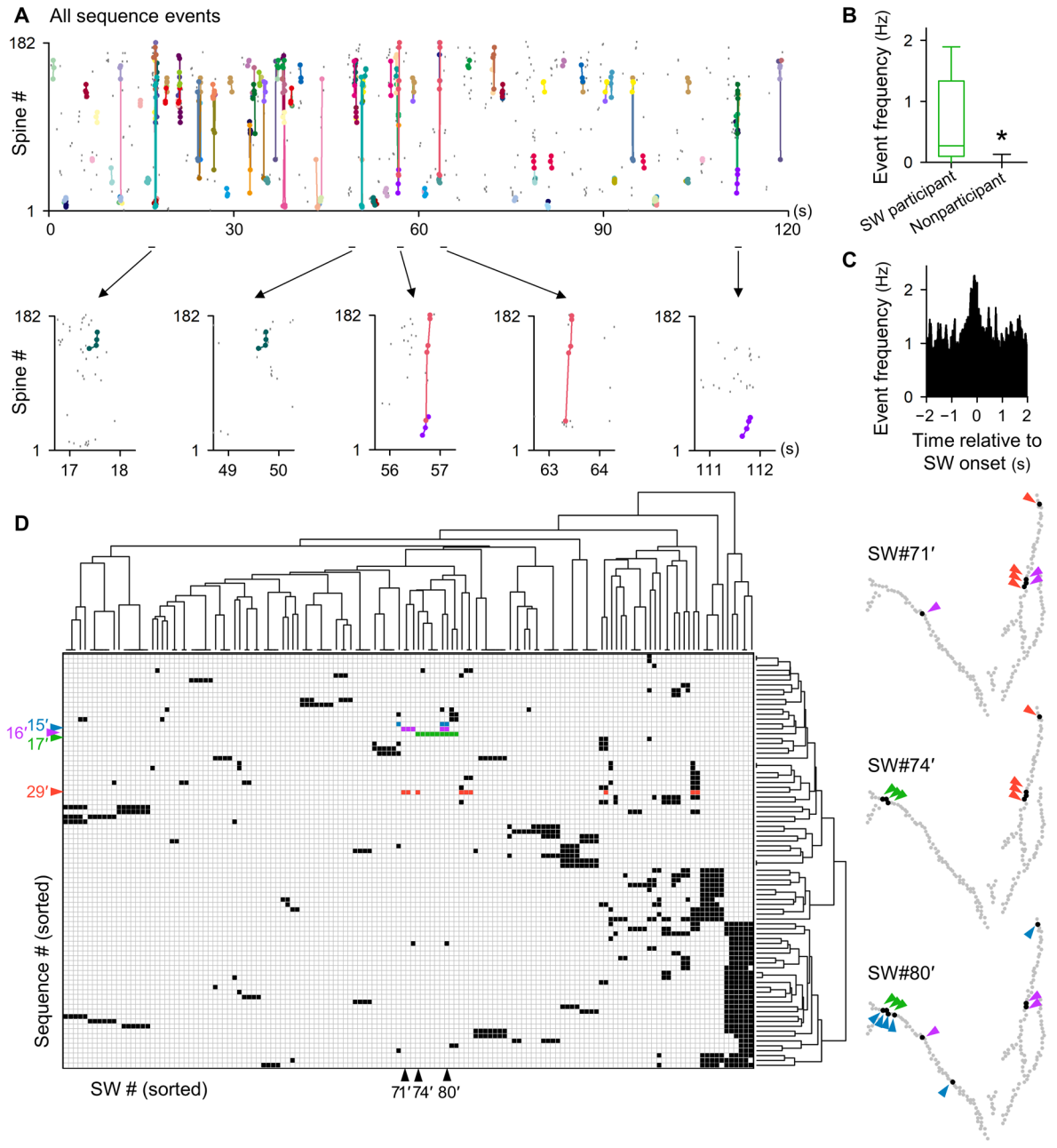

Fig. 3. SW participant cells receive a rich repertoire of repeated sequences of synaptic inputs during SWs. (**A**) All sequences detected in a representative raster plot are shown in different colors. Five sequences are temporally expanded (lower). (**B**) SW participants exhibited sequences more frequently than nonparticipants ($n = 14$ videos from 12 SW participants and $n = 9$ videos from 9 nonparticipants; $^*P = 0.0015$, $U = 14$, Mann-Whitney U test). (**C**) Peri-SW time histograms of the mean event frequency of sequences in 12 SW participants. (**D**) Representative combinatorial patterns of individual sequences participating in individual SWs (left). Sequences and SWs were individually sorted along their dendrogram based on Ward's method ($n = 143$ SW events and $n = 85$ sequences). Representative spatial distributions of spines involved in sequences #15′ (blue), #16′ (purple), #17′ (green), and #29′ (red), which were observed in SW events #71′, #74′, and #80′ (right).

we confirmed this positive correlation (fig. S4D). However, this regression line had a steeper slope than that of random surrogates, indicating that sequences were not passive consequences of increased synaptic activity but were actively produced by hippocampal microcircuits. Although calcium activity was more frequent in basal dendrites than in proximal apical dendrites ($P = 0.006$, $U = 5$, Mann-Whitney's U test), the event frequency of sequences did not differ between basal and proximal apical dendrites ($P = 0.056$, $t_{12} = 2.1$, Welch's t test).

We detected 313 sequences in 23 videos of 21 cells. On average, a single sequence consisted of 5.0 ± 1.9 spines (mean ± SD of 313 sequences, ranging from 3 to 14 spines) and repeated 2.4 ± 1.0 times (ranging from two to nine times) during the observation time. The median duration of a sequence was 129 ms (fig. S5A), and the median time interval between two consecutive spine activities in a sequence was 30 ms (fig. S5B). Synaptic activity onto a dendritic branch is nonlinearly summed at interactivity intervals between 0 and 40 ms (*27*).

We found that 59.5% of the spine activity pairs in sequences fell within this time window (fig. S5B). Highly active spines were not necessarily more frequently involved in sequences (fig. S6); that is, spines were recruited in sequences independent of their activity levels.

SW participants exhibited more sequences than nonparticipants (Fig. 3B; $P = 0.001$, $U = 13$, Mann-Whitney's U test), particularly during SWs (Fig. 3C). As described above, this increase in sequences during SWs cannot be explained by an increase in calcium activity during SWs (fig. S4D), indicating that sequential synaptic inputs occurred preferentially in SWs. Of a total of 726 repeats of 307 sequences in SW participants, 498 (68.6%) occurred during SWs. On average, a single SW event recruited 0.93 ± 2.6 sequences (mean ± SD of 1190 SWs from 12 videos of SW participants, ranging from 0 to 30 sequences). For visualization purposes, we sorted the orders of sequences and SWs independently using Ward's method–based hierarchical clustering and created a matrix that represents the combinatorial relationship of sequences and SWs (Fig. 3D). The matrix revealed that a sequence often participated in different SW events with different combinations of other sequences. The combinations of sequences were not fixed but seemed to vary flexibly over time.

Synaptic sequences converge on localized dendritic branches

To examine the spatial organization of each sequence (Fig. 4A), we calculated the geometric energy for the path distances between all pairs of spines participating in a sequence. The geometric energy was higher than the stochastic distribution estimated from 10,000 surrogates, in which the locations of spines were randomly exchanged within each video (Fig. 4B), suggesting that neighboring spines frequently participated in sequences. Another analysis also indicated that spines located within 10 μm of each other frequently co-participated in sequences (fig. S7). This finding applied to sequences during SWs and in the absence of SWs (fig. S7).

Sequences appeared to occur more heavily in some dendritic branches than in others (Fig. 4, A and C, left). To examine whether the loci where sequences occurred were spatially biased across dendritic trees, we calculated Shannon's entropy for the distributions of spines involved in sequences over dendritic branches as a function of the dendritic path distances from the cell bodies (Fig. 4C, right). In 83.3% of the 12 focal planes, the entropies, at least in part, took lower values than the chance level (fig. S8), suggesting that dendritic trees are heterogeneous in terms of receiving sequential synaptic inputs. This result seems consistent with anatomical studies showing that dendritic branches are structurally nonuniform in terms of synaptic connectivity and are functionally segmented (*8*, *28*, *29*).

Sequences vectorially activate adjacent spines along dendritic axes

We investigated the directionality of sequential spine activation along dendrites because somatic excitation may depend on whether the sequences occur toward or away from the cell body (*16*). In the following analyses, we focused on 350 local sequences that contained at least two spines at interspine distances of less than 10 μm, which were redefined from a total of 313 full-length sequences. To examine whether spines in a local sequence were serially activated along the longitudinal dendritic axis toward or away from the cell body, we plotted the spine locations against the spine activation times (Fig. 5A and fig. S9A). Because a local sequence was repeated at least twice, the time (x axis) and location (y axis) of each repeat were aligned to the centers of gravity of the spine activity. The plots were linearly regressed using the ordinary least-squares estimation. The coefficients of determination (R^2) were higher than the chance distribution of 10,000 bootstrapped surrogates (Fig. 5B). The same result was produced even by a nonparametric regression analysis in which only the orders of activity and location were plotted in the discrete system (fig. S9B). Thus, vector-like local activation of spines during sequences is a robust phenomenon.

The slopes (b_1) of the linear regression line were more positively or negatively biased than the chance distribution (Fig. 5C). In 188 (53.7%) of 350 local sequences, the b_1 values were negative; spines were serially activated toward the cell bodies (IN sequences). The remaining 157 (44.9%) sequences had positive b_1 values; spines were activated

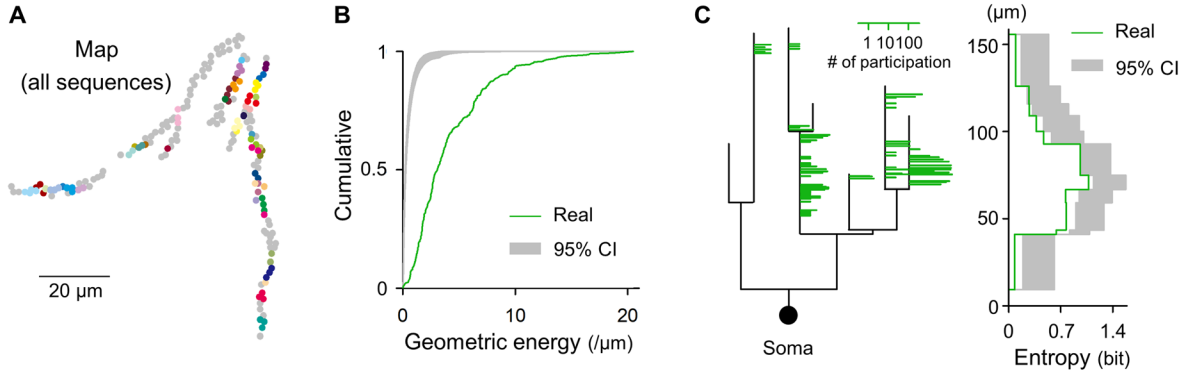

Fig. 4. Synaptic sequences appear nonuniformly in dendritic trees. (**A**) Locations of spines involved in a total of 76 sequences detected from a representative neuron are superimposed on the spine map. Each color indicates a single sequence. (**B**) The cumulative density function of the geometric energy (spatial clustering) of spines involved in individual sequences was compared to the 95% confidence interval (gray area) of its chance distribution estimated from 10,000 surrogates, in which the spine locations were randomly exchanged within the videos. All 313 sequences are pooled. (**C**) A topographic tree plot indicates the locations of spines that participated in sequences in a representative video. The heights of individual green bars on the tree represent the total number of events in sequences in which the corresponding spines participated. The ordinate indicates the path distance from the cell body. On the basis of this tree plot, we calculated entropy as the spatial bias of sequence-relevant spine activity across dendritic branches (right). The 95% confidence intervals (gray) were estimated from 10,000 surrogates, in which the numbers of sequence participations were randomly exchanged among the recorded spines.

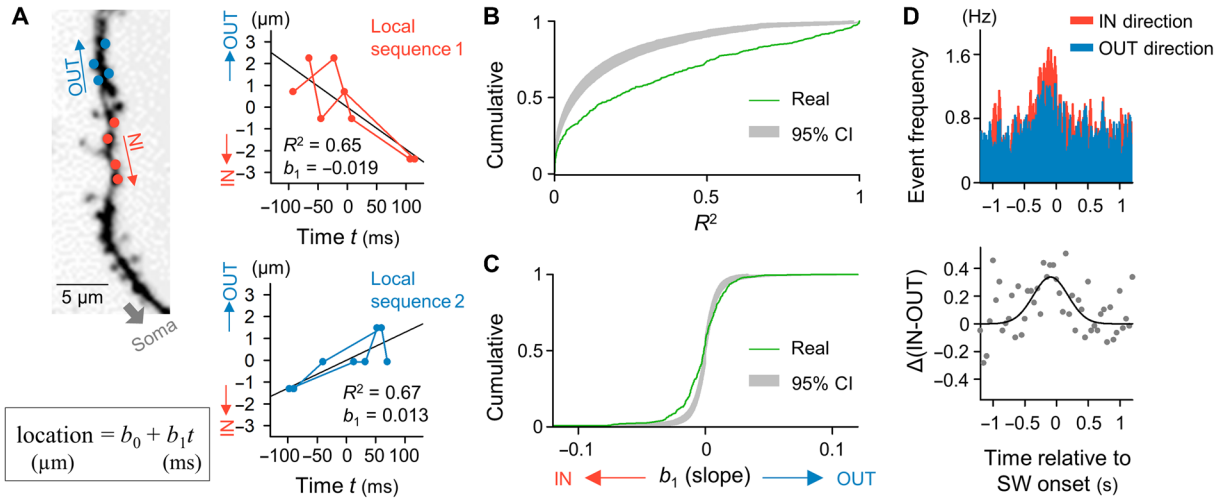

Fig. 5. Sequences vectorially activate adjacent spines in the IN or OUT directions along the dendritic axis. (**A**) Representative local sequences that had different directions, IN (inbound, red) and OUT (outbound, blue), relative to the cell body. Relative locations of the spines in these two local sequences are plotted as a function of relative times of their activity (*t*). In these coordinate planes, we calculated the coefficients of determination (R^2) and the slopes (b_1) of the regression lines (black). (**B** and **C**) The cumulative density functions of R^2 (B) and b_1 (C) of all 350 local sequences were compared to the 95% confidence intervals (gray areas) of 10,000 bootstrap surrogates. (**D**) Peri-SW time histograms of the event frequencies of IN (red) and OUT (blue) sequences (top) and their differences (bottom).

away from the cell bodies (OUT sequences). We plotted the time change in the event frequencies of IN and OUT sequences (Fig. 5D). IN sequences dominated OUT sequences during SWs, whereas IN and OUT sequences were numerically balanced at baseline.

Last, we analyzed calcium increases in dendritic shafts. When sequence-relevant calcium transients were observed in given spines, the dendritic shafts near the spines exhibited larger calcium transients than those for sequence-irrelevant spine activity (fig. S10A). These results suggest nonlinear dendritic summation during spine sequences. The amplitudes of calcium transients in dendritic shafts did not differ between the IN and OUT directions (fig. S10B).

DISCUSSION

We discovered that SW participants, more than nonparticipants, received increased excitatory synaptic inputs during SWs, apparently consistent with a recent study demonstrating that neurons that were activated during novel spatial exploration task exhibit larger intracellular depolarizations than exploration-irrelevant neurons (*30*). Our main finding is that synaptic inputs were composed of the sequential activation of local spines. As a result, the overall spatial clustering of active spines increased during SWs. Clustered inputs are known to facilitate nonlinear dendritic computations (*15*, *31*–*33*), including local dendritic spikes. Local dendritic spikes of CA1 pyramidal cells induce the formation of new place fields (*34*). Thus, our finding may partially explain local dendritic spikes (*34*) and nonlinear excitation-to-inhibition ratios in SW participants during SWs (*30*).

SW participants received more synaptic inputs immediately before SW onset than nonparticipants. Even in nonparticipants, spine activity increased approximately 400 ms before SW onset. We assume that network excitability in the entire hippocampus increased gradually before SWs, and therefore, nonparticipants also received an increasing number of spine activations before SWs. However, in nonparticipants, the input increase was interrupted for certain reasons, such as nonlinear summation or lateral inhibition. The idea of gradual increases in hippocampal network excitability is consistent with the fact that the geometric energy increased around the SW periods only in SW participants and that dendritic shafts near spines exhibited larger calcium increases when the spines participated in sequences. Clustered input-induced nonlinear dendritic summation may lead to action potentials in SW participants.

The sequential firing of multiple neurons has been demonstrated in multiple regions, including the hippocampus and other cortical regions (*1*–*7*); however, how postsynaptic neurons receive such spike sequences has not been clarified. In this regard, there were three possibilities: (i) Sequential spikes across different neurons are dispersedly transmitted to dendrites of different neurons, (ii) they are distributed to various dendritic trees of a neuron, or (iii) they converge onto the dendritic foci of a neuron. Our findings coincide with the third possibility: Spike sequences activate local dendrites. Moreover, we found two additional phenomena. First, multiple clustered spine sequences occurred simultaneously over different dendritic trees during a single SW event. Second, local spine activity formed vectorial sequences in either the IN or OUT direction. An optical manipulation study has demonstrated that even the same spine sets can differentially activate dendrites depending on whether their activation order is IN or OUT (*16*), suggesting that not only the spatial clustering but also the direction of local inputs could affect somatic excitation through nonlinear dendritic summation. In the hippocampus, a memory engram is replayed in either forward or reverse order (*35*, *36*), and it may excite a postsynaptic neuron differently depending on whether it is occurring in the IN or OUT direction (Fig. 6).

Attention must be paid to our data because we used hippocampal slice cultures whose microcircuits were partially reorganized without extrahippocampal afferents. CA1 pyramidal neurons in vivo receive excitatory synaptic inputs mainly from the CA3 region and the entorhinal cortex. When the hippocampus is obliquely sliced, afferent fibers from the CA3 region are more likely to be preserved (*30*). Because the surgical isolation of CA3 abolishes the generation of SWs in these slices, SWs in our slice preparations are of CA3 origin. In

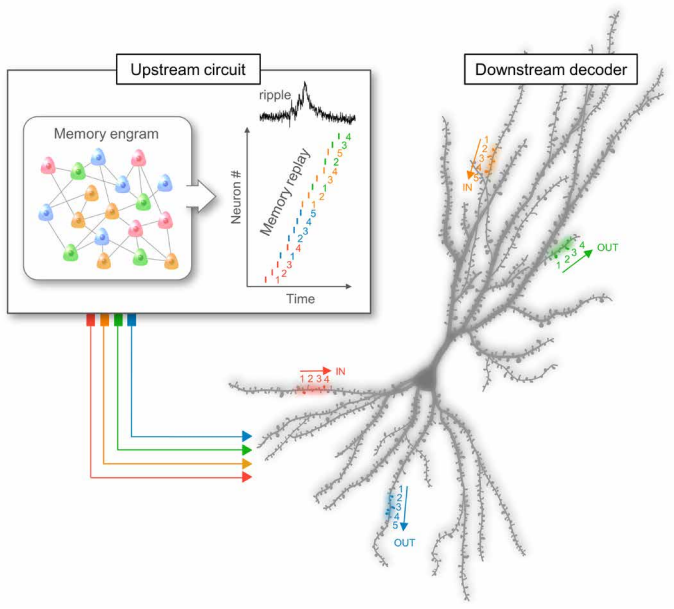

Fig. 6. Distributed clusters of sequential synaptic activation during SWs. During activity propagation in SWs, sequential spikes are sorted into discrete sequential synaptic inputs to locally clustered spines of a downstream neuron. The sequential synaptic inputs are vectorially toward (IN) or away from (OUT) the cell body. Thus, sequential replays of neuronal ensembles may converge on specific target dendritic zones (hotspots) in a spatiotemporally preserved fashion, thereby augmenting nonlinear dendritic computation.

the present study, the observation of calcium activity was limited to spines located within 200 μm of the cell bodies, where CA1 pyramidal neurons receive synaptic inputs from the CA3 region. Dendrites and their primary branches, as well as spine densities, of CA1 pyramidal cells develop in a similar manner in both cultured hippocampal slices and in vivo hippocampus (*37*). Therefore, although slice cultures do not perfectly replicate the in vivo situation, the basic structures of hippocampal CA3-to-CA1 circuits are largely preserved after rewiring without extrahippocampal afferent inputs. We believe that this ex vivo preservation renders the biophysical basis for sequential spikes ex vivo, although they do not represent memory replays of awake experiences. This notion may lead to an extended idea that self-organized "default" microcircuits are intrinsically wired to emit locally sequential synaptic inputs during neuronal synchronization. Our findings suggest that neurons are intrinsically programmed to elaborate upon subcellularly precise circuits that support the sequential activation of adjacent spines.

We observed multiple, simultaneous spine sequences during SWs that were recruited flexibly in different SWs. The complex dynamics of spine activity may signify a subcellular mechanism that associatively integrates discrete hippocampal information. We posit that spine sequences represent temporal modules of dendritic inputs; that is, dendrites are compartmentalized into building blocks for neuronal excitation (*33*) that receive orthogonally segmented activity from upstream cell assemblies during SWs (*6*, *7*). Thus, sequential replays of neuronal ensembles may converge on specific target dendritic zones (hotspots) in a spatiotemporally preserved fashion, thereby augmenting nonlinear dendritic computation.

MATERIALS AND METHODS

Ethical approval and animals

Experiments were performed with the approval of the animal experiment ethics committee at the University of Tokyo (approval nos. P29-2 and P29-3) and adhered to the University of Tokyo guidelines for the care and use of laboratory animals. Wistar/ST (SLC, male or female) rats were housed in cages under standard laboratory conditions (12-hour light:12-hour dark cycle, ad libitum access to food and water). All efforts were made to minimize the animals' suffering and the number of animals used.

Drugs

Carbachol was dissolved at 10 mM in water and stored at 4°C. Immediately before use, the stock solution was diluted to 10 μM in artificial cerebrospinal fluid (aCSF) that consisted of 127 mM NaCl, 26 mM $NaHCO_3$, 3.5 mM KCl, 1.24 mM NaH_2PO_4, 1.3 mM $MgSO_4$, 2.4 mM $CaCl_2$, 10 mM glucose, and 0.4 mM Trolox.

Slice culture preparations

Entorhinal-hippocampal organotypic slices were prepared from Wistar/ST rats on postnatal day 7 as previously described (*38*). Rat pups were anesthetized with hypothermia and isoflurane and were subsequently decapitated. The brains were removed and placed in ice-cold oxygenated Gey's balanced salt solution supplemented with 25 mM glucose. The brains were sliced horizontally (300 μm thick) using a vibratome, and the entorhinal-hippocampal regions were trimmed using a surgical microknife. The slices were placed on Omnipore membrane filters and incubated in 5% CO_2 at 35°C. The culture medium, which was composed of 50% minimal essential medium, 25% Hanks' balanced salt solution, 25% horse serum, and antibiotics, was changed every 3.5 days. Experiments were performed at 9 to 18 days in vitro.

LFP recording

Slices were mounted in a recording chamber and perfused at a rate of 1.5 to 3 ml/min (32° to 33°C) with oxygenated aCSF. SWs were recorded using a borosilicate glass pipette (1 to 2 megohms) filled with aCSF, which was carefully placed in the CA1 pyramidal layer within a distance of 50 μm from a patch-clamp pipette. Electrophysiological signals were low pass–filtered at 2 kHz and digitized at 20 kHz. The traces were denoised using the Okada filter (*39*) and bandpass-filtered between 2 and 30 Hz to detect SWs. SWs were detected at a threshold of 7 × SD of the baseline noise level. Then, the peak times during the SW events were determined, and the LFP inflection points before the peak times were defined as the SW onset times. The detected events were visually scrutinized and manually rejected if they were erroneously detected. To characterize the LFP signals in a time-frequency domain, we further convoluted the LFP signals with a Morlet wavelet family. For analyses of current source density, one electrode was placed in the CA1 stratum pyramidale, while another electrode was placed serially in the stratum lacunosum moleculare, the stratum radiatum, or the stratum oriens. Current source densities for the averaged LFP traces of 20 consecutive SWs were computed using the cubic spline method at a 150-μm step (*40*) and smoothed using a Gaussian filter ($\sigma = 2$). To examine the effect of carbachol perfusion on the event frequency of SWs, we recorded baseline LFP traces from the CA1 stratum pyramidale for 10 min; then, 10 μM carbachol was bath-applied. LFP traces during carbachol perfusion were recorded from 10 to 20 min after the initiation of the perfusion.

Calcium imaging from spines

Hippocampal CA1 pyramidal neurons in the superficial layer were patch-clamped using glass pipettes (3.5 to 6 ohms) filled with a solution containing the following components: 47.7 mM $CsMeSO_4$, 92.3 mM CsCl, 10 mM Hepes, 10 mM phosphocreatine, 4 mM MgATP, 0.3 mM NaGTP, and 0.2 mM Fluo-4. Whole-cell recordings were preceded by cell-attached recordings for 1 to 2 min to classify SW participants and nonparticipants. The membrane potential was voltage-clamped at −30 mV, because calcium entry into spines was mediated mainly by NMDA receptor channels (*11*, *23*). Time-series images were acquired at 100 frames per second using a Nipkow disk confocal unit, a complementary metal oxide semiconductor camera, and a water immersion objective lens (60×, 1.0 numerical aperture). The fluorophore was excited using a 488-nm laser at 0.2 to 0.3 mW and visualized using a 500-nm longpass emission filter. To avoid a space clamp problem, we monitored only spines located within 200 μm of the cell bodies. At the end of each experiment, stereoscopic images were captured at a *Z* step of 1 μm at 1 frame per second, and spines, their dendritic shafts, and the morphology of the dendrites were three-dimensionally measured.

Calcium activity detection in spines and dendritic shafts

For all dendritic spines imaged on a confocal plane, regions of interest (ROIs) were placed manually using custom software in Microsoft Visual Basic (*2*). The diameter of each ROI was tailored to the visible size of the dendritic spine. ROIs for the dendritic shafts were determined manually on the root of the spines recruited in the local sequences. The average fluorescence intensity in each ROI was calculated at each video frame and was used to determine the fluorescence change ($\Delta F/F$). The $\Delta F/F$ value was calculated as $(F_t - F_0)/F_0$, where F_t is the fluorescence intensity at frame time t and F_0 is the baseline, which was calculated as the average of the minimal 3% values in the fluorescence intensities during a period of ±5 s relative to time t. Shot noise was removed using the Okada filter (*39*). Transient calcium activity was detected using optimized machine learning as described elsewhere (*41*). Calcium transients were detected at a threshold of 5 × SD of the baseline noise level. Baseline noise levels were determined on training data that contained typical traces of 10 noise samples and on the calcium trace of each spine. The detection algorithm assumed that the data had characteristics of white Gaussian noise with unequal powers across the dataset. To detect calcium transients, 20 typical calcium transients were used for training. After detecting the peak times of calcium transients using the machine learning algorithm, the onset times were defined as the inflection points before the peak times. We regarded these onset times as the times when the calcium events occurred. The amplitudes of calcium transients were calculated as the difference of the fluorescence intensities between the onset and peak times. To avoid the influence of photobleaching and phototoxicity, we analyzed the recording time during which the event frequency of calcium activity was not significantly reduced from the frequency for the first 10 s of the recordings (up to 120 s).

We defined SW-relevant spikes as spikes that occurred within ±20 ms of the SW onset and SW-relevant spine activity as activity that occurred within 300 ms before the SW onset according to the triggered average histogram of the spike rates and the spine activity rates. We classified neurons that had higher participation rates, i.e., the probabilities that SWs were accompanied by spikes of a given neuron, compared to 95% confidence intervals of their chance levels as participants. Chance level was estimated from 10,000 surrogates, in which the Poisson point process generated the same number of spikes in each cell.

Detection of the sequential activity of spines

The spatiotemporal activity pattern of C spines (all spines from an experiment) for N_{all} frames can be represented as a $C \times N_{all}$ matrix, in which frames without or with calcium activity are denoted as 0 or 1, respectively. Calcium activity (i.e., the value 1) was smoothed using the Gaussian filter (σ = 4 frames; i.e., 40 ms); then, the raster plot was segmented into a series of $C \times N_t$ matrices, where N_t is the window length (time bins = 30 frames; i.e., 300 ms) at a given time point t. The correspondence of spine activity at two time points m and n was evaluated using the sum of all the elements of the Hadamard products of the $C \times N_m$ and $C \times N_n$ matrices (*26*). Under our conditions, the element sum is 14.1795 when the activity of two spines is repeated exactly with the same timings. Therefore, we adopted this value as a threshold for sequence detection; that is, one sequence contained at least three spines and was repeated at least twice. Spines that were activated in both $C \times N_m$ and $C \times N_n$ matrices were defined as spines that participated in sequences. To avoid duplicate detections of the same pairs of repeated sequence events, we considered only the matrix pair whose Hadamard product's element sums exhibited the local maximal value. Sequences of which parts were completely identical were not distinguished and were counted as the repetition of a single sequence.

Geometric energy

The locations of spines were three-dimensionally determined post hoc, and interspine distances (i.e., path lengths along the longitudinal dendritic axes) were measured for all possible pairs of spines synchronized at time t (Fig. 2, K and L) or spines participating in a sequence (Fig. 4B). Then, $\Sigma 1/d_{ij}$ was calculated as the geometric energy (E_g), where d_{ij} is the interspine distance between spines i and j (*25*). E_g was compared with the chance level estimated from 10,000 surrogates, in which the locations of spines were randomly replaced with the locations of other spines within the video.

To confirm the spatial clustering of coactivated spines, we counted the number of spine pairs of simultaneously activated spines that were located within 10 μm of each other at time t (fig. S3) or counted spine pairs participating in a sequence (fig. S7). The number of coactive spine pairs was compared with the chance level estimated from 10,000 surrogates, in which the locations of spines were randomly replaced with those of other spines within the video.

Entropy

To estimate the spatial bias of sequence-relevant spines over dendritic trees, we calculated Shannon's entropies for the distributions of sequence-participating spines across different dendritic branches as a function of the path distances from the cell bodies.

$$H = \Sigma \{(n_i/N) \log (n_i/N)\}$$

where n_i is the sum of the participating sequences of spine i located farther from a given branch point and N is the sum of the participating sequences of all recorded spines located farther from the same branch point. The distribution of the entropy was compared with the chance level estimated from 10,000 surrogates, in which the locations of spines are exchanged with the locations of other spines. The entropy quantifies the randomness of the distribution; thus, its value is lower when spines are more localized in specific branches.

Dendrogram

When C sequences and N SWs are detected in a video, combinatorial patterns of individual sequences participating in individual SWs are represented as a $C \times N$ matrix. In the matrix, a given element in which the sequence participates in the SW is denoted as 1; otherwise, it is 0. To sort the $C \times N$ matrix according to the participation similarity of individual sequences or SWs, we used agglomerative hierarchical clustering. The similarities were evaluated by the inner products of pairs of rows (or pairs of columns), which create the $C \times C$ (or $N \times N$) matrices. Dendrograms were depicted using Ward's method based on the within-cluster sum of squares as follows

$$d(r,s) = \sqrt{\frac{2 n_r n_s}{(n_r + n_s)}} \|x_r - x_s\|^2$$

where x_r and x_s are the centroids of cluster r and s, n_r and n_s are the number of elements in clusters r and s, and $||x_r - x_s||^2$ indicates the Euclidean distance between x_r and x_s.

Direction of sequences

We defined a local sequence as a part of a sequence in which any pair of spines had an interspine distance of less than 10 μm. To examine whether local sequences had directions, we used two types of regression models: linear regression and nonparametric regression. In the linear regression model, we plotted the spine locations against the spine activity times aligned with the center of gravity of the spine activity in each repetition of the local sequences on a coordinate plane. We calculated the coefficients of determination (R^2) and the slopes (b_1) of the regression lines (location = $b_0 + b_1 t$) using the ordinary least-squares estimation in the coordinated plane. In the nonparametric regression model, we plotted the spine location order against the spine activity order in the discrete system and calculated R^2 of the regression line using the nonparametric regression method. The chance levels of R^2 and b_1 were estimated from 10,000 bootstrapped surrogates, in which the locations of spines in a local sequence were randomly resampled within the local sequence, while the activity times were fixed. Local sequences that had negative and positive slopes (b_1) were regarded as sequences that were vectorially activated toward the cell bodies (IN) or away from the cell bodies (OUT), respectively. The differences in the event frequencies of IN and OUT sequences during SWs were calculated in the time bins of five frames (i.e., 50 ms) and fit using a Gaussian model.

Data analysis

Pooled data are reported as the means ± SD or as box-and-whisker plots composed of the medians (central line in the box), 25th and 75th percentiles (box), and 10th and 90th percentiles (whiskers).

SUPPLEMENTARY MATERIALS

Supplementary material for this article is available at http://advances.sciencemag.org/cgi/content/full/6/7/eaay1492/DC1

Fig. S1. Some, but not all, CA1 neurons emit SW-locked spikes.
Fig. S2. Spontaneous calcium transients are recorded simultaneously from multiple spines in a single neuron in a SW-emitting slice.
Fig. S3. SW participants receive spatially clustered spine activity during SWs.
Fig. S4. Sequential spine activity appeared more frequently than the chance level in SW participants.
Fig. S5. Temporal properties of sequential spine activity.
Fig. S6. Spines are recruited in sequences independent of their calcium activity frequency.
Fig. S7. Sequential spine activity is spatially clustered irrespective of the occurrence of SWs.
Fig. S8. Spines involved in sequence are localized in specific dendritic branches.
Fig. S9. Directionality of local sequences: Nonparametric analysis.
Fig. S10. Sequential spine activity induces larger calcium transients in nearby dendritic shafts.
Movie S1. Time-lapse confocal imaging of calcium activity from spines.

REFERENCES AND NOTES

1. A. J. Peters, S. X. Chen, T. Komiyama, Emergence of reproducible spatiotemporal activity during motor learning. *Nature* **510**, 263–267 (2014).
2. Y. Ikegaya, G. Aaron, R. Cossart, D. Aronov, I. Lampl, D. Ferster, R. Yuste, Synfire chains and cortical songs: Temporal modules of cortical activity. *Science* **304**, 559–564 (2004).
3. C. D. Harvey, P. Coen, D. W. Tank, Choice-specific sequences in parietal cortex during a virtual-navigation decision task. *Nature* **484**, 62–68 (2012).
4. A. K. Lee, M. A. Wilson, Memory of sequential experience in the hippocampus during slow wave sleep. *Neuron* **36**, 1183–1194 (2002).
5. A. D. Grosmark, G. Buzsaki, Diversity in neural firing dynamics supports both rigid and learned hippocampal sequences. *Science* **351**, 1440–1443 (2016).
6. A. Malvache, S. Reichinnek, V. Villette, C. Haimerl, R. Cossart, Awake hippocampal reactivations project onto orthogonal neuronal assemblies. *Science* **353**, 1280–1283 (2016).
7. B. E. Pfeiffer, D. J. Foster, Autoassociative dynamics in the generation of sequences of hippocampal place cells. *Science* **349**, 180–183 (2015).
8. S. Druckmann, L. Feng, B. Lee, C. Yook, T. Zhao, J. C. Magee, J. Kim, Structured synaptic connectivity between hippocampal regions. *Neuron* **81**, 629–640 (2014).
9. M. F. Iacaruso, I. T. Gasler, S. B. Hofer, Synaptic organization of visual space in primary visual cortex. *Nature* **547**, 449–452 (2017).
10. T. Kleindienst, J. Winnubst, C. Roth-Alpermann, T. Bonhoeffer, C. Lohmann, Activity-dependent clustering of functional synaptic inputs on developing hippocampal dendrites. *Neuron* **72**, 1012–1024 (2011).
11. N. Takahashi, K. Kitamura, N. Matsuo, M. Mayford, M. Kano, N. Matsuki, Y. Ikegaya, Locally synchronized synaptic inputs. *Science* **335**, 353–356 (2012).
12. Z. F. Mainen, T. J. Sejnowski, Influence of dendritic structure on firing pattern in model neocortical neurons. *Nature* **382**, 363–366 (1996).
13. M. Migliore, G. M. Shepherd, Emerging rules for the distributions of active dendritic conductances. *Nat. Rev. Neurosci.* **3**, 362–370 (2002).
14. A. Reyes, Influence of dendritic conductances on the input-output properties of neurons. *Annu. Rev. Neurosci.* **24**, 653–675 (2001).
15. A. Losonczy, J. C. Magee, Integrative properties of radial oblique dendrites in hippocampal CA1 pyramidal neurons. *Neuron* **50**, 291–307 (2006).
16. T. Branco, B. A. Clark, M. Häusser, Dendritic discrimination of temporal input sequences in cortical neurons. *Science* **329**, 1671–1675 (2010).
17. G. Girardeau, K. Benchenane, S. I. Wiener, G. Buzsáki, M. B. Zugaro, Selective suppression of hippocampal ripples impairs spatial memory. *Nat. Neurosci.* **12**, 1222–1223 (2009).
18. H. Norimoto, K. Makino, M. Gao, Y. Shikano, K. Okamoto, T. Ishikawa, T. Sasaki, H. Hioki, S. Fujisawa, Y. Ikegaya, Hippocampal ripples down-regulate synapses. *Science* **359**, 1524–1527 (2018).
19. K. Okamoto, T. Ishikawa, R. Abe, D. Ishikawa, C. Kobayashi, M. Mizunuma, H. Norimoto, N. Matsuki, Y. Ikegaya, Ex vivo cultured neuronal networks emit in vivo-like spontaneous activity. *J. Physiol. Sci.* **64**, 421–431 (2014).
20. K. Matsumoto, T. Ishikawa, N. Matsuki, Y. Ikegaya, Multineuronal spike sequences repeat with millisecond precision. *Front. Neural. Circuits* **7**, 112 (2013).
21. N. Takahashi, T. Sasaki, W. Matsumoto, N. Matsuki, Y. Ikegaya, Circuit topology for synchronizing neurons in spontaneously active networks. *Proc. Natl. Acad. Sci. U.S.A.* **107**, 10244–10249 (2010).
22. G. Buzsáki, Hippocampal sharp wave-ripple: A cognitive biomarker for episodic memory and planning. *Hippocampus* **25**, 1073–1188 (2015).
23. C. Kobayashi, K. Okamoto, Y. Mochizuki, H. Urakubo, K. Funayama, T. Ishikawa, T. Kashima, A. Ouchi, A. F. Szymanska, S. Ishii, Y. Ikegaya, GABAergic inhibition reduces the impact of synaptic excitation on somatic excitation. *Neurosci. Res.* **146**, 22–35 (2018).
24. B. K. Hulse, L. C. Moreaux, E. V. Lubenov, A. G. Siapas, Membrane potential dynamics of CA1 pyramidal neurons during hippocampal ripples in awake mice. *Neuron* **89**, 800–813 (2016).
25. K. Makino, K. Funayama, Y. Ikegaya, Spatial clusters of constitutively active neurons in mouse visual cortex. *Anat. Sci. Int.* **91**, 188–195 (2016).
26. K. Louie, M. A. Wilson, Temporally structured replay of awake hippocampal ensemble activity during rapid eye movement sleep. *Neuron* **29**, 145–156 (2001).
27. A. Polsky, B. W. Mel, J. Schiller, Computational subunits in thin dendrites of pyramidal cells. *Nat. Neurosci.* **7**, 621–627 (2004).
28. G. Yang, C. S. Lai, J. Cichon, L. Ma, W. Li, W.-B. Gan, Sleep promotes branch-specific formation of dendritic spines after learning. *Science* **344**, 1173–1178 (2014).
29. K. S. Lee, K. Vandemark, D. Mezey, N. Shultz, D. Fitzpatrick, Functional synaptic architecture of callosal inputs in mouse primary visual cortex. *Neuron* **101**, 421–428.e5 (2019).

30. M. Mizunuma, H. Norimoto, K. Tao, T. Egawa, K. Hanaoka, T. Sakaguchi, H. Hioki, T. Kaneko, S. Yamaguchi, T. Nagano, N. Matsuki, Y. Ikegaya, Unbalanced excitability underlies offline reactivation of behaviorally activated neurons. *Nat. Neurosci.* **17**, 503–505 (2014).
31. N. L. Golding, N. P. Staff, N. Spruston, Dendritic spikes as a mechanism for cooperative long-term potentiation. *Nature* **418**, 326–331 (2002).
32. J. Schiller, G. Major, H. J. Koester, Y. Schiller, NMDA spikes in basal dendrites of cortical pyramidal neurons. *Nature* **404**, 285–289 (2000).
33. A. Losonczy, J. K. Makara, J. C. Magee, Compartmentalized dendritic plasticity and input feature storage in neurons. *Nature* **452**, 436–441 (2008).
34. M. E. J. Sheffield, M. D. Adoff, D. A. Dombeck, Increased prevalence of calcium transients across the dendritic arbor during place field formation. *Neuron* **96**, 490–504.e5 (2017).
35. D. J. Foster, M. A. Wilson, Reverse replay of behavioural sequences in hippocampal place cells during the awake state. *Nature* **440**, 680–683 (2006).
36. K. Diba, G. Buzsáki, Forward and reverse hippocampal place-cell sequences during ripples. *Nat. Neurosci.* **10**, 1241–1242 (2007).
37. A. De Simoni, C. B. Griesinger, F. A. Edwards, Development of rat CA1 neurones in acute versus organotypic slices: Role of experience in synaptic morphology and activity. *J. Physiol.* **550**, 135–147 (2003).
38. R. Koyama, R. Muramatsu, T. Sasaki, R. Kimura, C. Ueyama, M. Tamura, N. Tamura, J. Ichikawa, N. Takahashi, A. Usami, M. K. Yamada, N. Matsuki, Y. Ikegaya, A low-cost method for brain slice cultures. *J. Pharmacol. Sci.* **104**, 191–194 (2007).
39. M. Okada, T. Ishikawa, Y. Ikegaya, A computationally efficient filter for reducing shot noise in low S/N data. *PLOS ONE* **11**, e0157595 (2016).
40. S. de Marie, J. H. Hoeijmakers, J. T. Poolman, H. C. Zanen, Filter radioimmunoassay, a method for large-scale serotyping of Neisseria meningitidis. *J. Clin. Microbiol.* **20**, 255–258 (1984).
41. A. F. Szymanska, C. Kobayashi, H. Norimoto, T. Ishikawa, Y. Ikegaya, Z. Nenadic, Accurate detection of low signal-to-noise ratio neuronal calcium transient waves using a matched filter. *J. Neurosci. Methods* **259**, 1–12 (2016).

Acknowledgments
Funding: This work was supported by JST ERATO (JPMJER1801), JSPS Grants-in-Aid for Scientific Research (18H05525 and 17H07086), the Sasakawa Scientific Research Grant from the Japan Science Society (2018-4008), and the Human Frontier Science Program (RGP0019/2016). This work was conducted partially as a program at the International Research Center for Neurointelligence (WPI-IRCN) of The University of Tokyo Institutes for Advanced Study at The University of Tokyo. **Author contributions:** T.I. and Y.I. designed and implemented the study and wrote the manuscript. T.I. performed the experiments. T.I. and Y.I. analyzed the data and discussed the results. **Competing interests:** The authors declare that they have no competing interests. **Data and materials availability:** All data needed to evaluate the conclusions in the paper are present in the paper and/or the Supplementary Materials. Additional data related to this paper may be requested from the authors.

Submitted 23 May 2019
Accepted 2 December 2019
Published 12 February 2020
10.1126/sciadv.aay1492

Citation: T. Ishikawa, Y. Ikegaya, Locally sequential synaptic reactivation during hippocampal ripples. *Sci. Adv.* **6**, eaay1492 (2020).

Science Advances

Locally sequential synaptic reactivation during hippocampal ripples

Tomoe Ishikawa and Yuji Ikegaya

Sci Adv **6** (7), eaay1492.
DOI: 10.1126/sciadv.aay1492